Residual Circulation and Tropopause Structure

THOMAS BIRNER

Department of Physics, University of Toronto, Toronto, Ontario, Canada, and Department of Atmospheric Science, Colorado State University, Fort Collins, Colorado

(Manuscript received 14 August 2009, in final form 16 March 2010)

ABSTRACT

The effect of large-scale dynamics as represented by the residual mean meridional circulation in the transformed Eulerian sense, in particular its stratospheric part, on lower stratospheric static stability and tropopause structure is studied using a comprehensive chemistry–climate model (CCM), reanalysis data, and simple idealized modeling. Dynamical forcing of static stability as associated with the vertical structure of the residual circulation results in a dominant dipole forcing structure with negative static stability forcing just below the tropopause and positive static stability forcing just above the tropopause. This dipole forcing structure effectively sharpens the tropopause, especially during winter. Furthermore, the strong positive lowermost stratospheric static stability forcing causes a layer of strongly enhanced static stability just above the extratropical tropopause—a tropopause inversion layer (TIL)—especially in the winter midlatitudes. The strong positive static stability forcing is shown to be mainly due to the strong vertical gradient of the vertical residual velocity found just above the tropopause in the winter midlatitudes.

Stratospheric radiative equilibrium (SRE) solutions are obtained using offline radiative transfer calculations for a given tropospheric climate as simulated by the CCM. The resulting tropopause height in SRE is reduced by several kilometers in the tropics but is increased by 1–2 km in the extratropics, strongly reducing the equator-to-pole contrast in tropopause height. Moreover, the TIL in winter midlatitudes disappears in the SRE solution in contrast to the polar summer TIL, which stays intact. When the SRE solution is modified to include the effect of stratospheric dynamics as represented by the stratospheric residual circulation, the TIL in winter midlatitudes is recovered, suggesting that the static stability forcing associated with the stratospheric residual circulation represents the main cause for the TIL in the winter midlatitudes whereas radiation seems dominant in causing the polar summer TIL.

1. Introduction

The height of the tropopause is often considered to be set primarily by the combined effects of a dynamically active troposphere and a stratosphere in near-radiative equilibrium (e.g., Manabe and Strickler 1964; Held 1982; Thuburn and Craig 1997; Schneider 2007). Held (1982) introduced the concept of separating dynamical and radiative constraints to determine tropopause height. In one form of this concept, one assumes a given surface temperature and (constant) tropospheric lapse rate and obtains the height of the tropopause such that the temperature profile at and above the tropopause is in radiative equilibrium (Thuburn and Craig 2000). Provided a dynamical constraint exists that relates tropospheric lapse rate and tropopause height for given surface temperature, one has a closed problem to be solved for the tropospheric lapse rate and tropopause height simultaneously (Schneider 2007). The basic dependence of tropopause height on surface temperature and tropospheric lapse rate in this concept, among other things, provides a qualitative explanation for the observed equator-to-pole contrast in tropopause height (see above references).

In the tropics moist convection tends to constrain tropospheric lapse rates to a moist adiabat, at least in the middle to upper troposphere (Folkins and Martin 2005). The classical radiative–convective equilibrium model, which assumes a fixed tropospheric lapse rate set by convection, therefore predicts a tropopause as the upper boundary of the convectively adjusted region with an overlying stratosphere in radiative equilibrium (e.g., Manabe and Wetherald 1967). Note, however, that the tropopause, when defined as the coldest point in the

Corresponding author address: Thomas Birner, Department of Atmospheric Science, Colorado State University, 1371 Campus Delivery, Fort Collins, CO 80523.
E-mail: thomas@atmos.colostate.edu

DOI: 10.1175/2010JAS3287.1

© 2010 American Meteorological Society

temperature profile, may be well separated from the top of convection in these radiative–convective equilibrium models (Thuburn and Craig 2002). In the extratropics baroclinic eddies take over the role to adjust the tropospheric lapse rate (Haynes et al. 2001) and provide a dynamical constraint (e.g., Schneider 2004), even though convection might still play a role there (Juckes 2000; Frierson et al. 2006).

A stratosphere in radiative equilibrium clearly represents an idealization. Stratospheric dynamics, as represented by the stratospheric residual circulation, provides adiabatic cooling near the tropical tropopause and lower stratosphere, which tends to raise the tropical tropopause out of reach of convection (e.g., Highwood and Hoskins 1998) and therefore contributes to form the so-called tropical tropopause layer (TTL). Near the extratropical tropopause and lower stratosphere the stratospheric residual circulation provides adiabatic warming, which tends to lower the extratropical tropopause. That is, the equator-to-pole contrast in tropopause height is at least partially due to the stratospheric dynamics (Kirk-Davidoff and Lindzen 2000). A stronger stratospheric circulation leads to a larger equator-to-pole contrast in tropopause height and a weaker circulation leads to a smaller contrast (Thuburn and Craig 2000; Wong and Wang 2003). The present study finds that more than half of the equator-to-pole contrast in tropopause height is due to stratospheric dynamics. Moreover, the separation of the top of convection and the tropopause in the tropics, that is, the existence of the TTL, is found to be almost entirely due to stratospheric dynamics. Stratospheric dynamics also significantly impacts tropopause height variability on intraseasonal (Son et al. 2007) and interannual (e.g., Zhou et al. 2001) time scales, while stratospheric processes play a crucial role in future tropopause height trends (Son et al. 2009).

Another limitation of stratospheric radiative equilibrium (SRE) is that it fails to predict the observed lower stratospheric static stability structure. In particular, the midlatitudinal isothermal lower stratospheric stratification in SRE (cf. Thuburn and Craig 2002) stands in contrast to the recently described marked stratification maximum just above the tropopause—the tropopause inversion layer (TIL) (Birner et al. 2002; Birner 2006; Randel et al. 2007b; Bell and Geller 2008; Bian and Chen 2008). However, processes that form and maintain this TIL are presently not well understood. Birner et al. (2002) speculated that warming due to lower stratospheric subsidence could play a role in forming a TIL at midlatitudes. [They also presumed that tropospheric eddies would lead to a relative cooling at tropopause level due to tropopause lifting, which was intended to describe the observed negative correlation between tropopause height and temperature (e.g., Zängl and Wirth 2002) but is somewhat misleading given that tropospheric eddies tend to warm the upper troposphere.] Wirth (2003, 2004) suggested that the asymmetry between upper-level cyclones and anticyclones and their effects on the local stratification around the tropopause is responsible for the existence of a TIL in the climatological mean, and Wirth and Szabo (2007) and A. R. Erler and V. Wirth (2009, unpublished manuscript) tested this idea in idealized baroclinic life cycle experiments. Randel et al. (2007b) pointed out that the lowermost stratospheric structure of water vapor and ozone resulting from stratosphere–troposphere exchange (STE) events has a radiative feedback such as to enhance stratification just above the tropopause, that is, to create a TIL (see also Kunz et al. 2009). It should be noted that this radiative mechanism inherently includes transport effects by assuming that the dynamics involved in the STE eventually lead to the observed water vapor and ozone distributions in the lowermost stratosphere (e.g., Pan et al. 1997, 2000; Hoor et al. 2002; Hegglin et al. 2006, 2009). Evidence that the radiative mechanism might not be the only mechanism at work to form a TIL comes from mechanistic dry core general circulation model (GCM) experiments that spontaneously form a TIL (Son and Polvani 2007). These experiments represent forced–dissipative equilibrium scenarios where the forcing mimics radiation and is represented by simple Newtonian relaxation and only large-scale dry dynamics are considered. That is, potential radiative effects due to dynamically created structures in radiative tracers such as water vapor and ozone are excluded. Finally, GCM simulations with a comprehensive chemistry–climate model (CCM) also exhibit a TIL of realistic strength and seasonal structure, even though of somewhat unrealistic vertical location and extent, presumably due to limited vertical resolution (Birner et al. 2006) combined with uncertainties in the precise location of the tropopause (Bell and Geller 2008).

In the present study it is asked to what extent large-scale stratospheric dynamics are responsible for the lower stratospheric static stability structure and the equator-to-pole contrast in tropopause height. Our approach is based on the assumption that ultimately the net effect of large-scale dynamics is represented by the residual mean meridional circulation in the transformed Eulerian mean (TEM) sense (Andrews et al. 1987) and its meridional and vertical structure (which determines meridional and vertical residual velocities).

Results based on simulations with a comprehensive chemistry–climate model [essentially the same as in Birner et al. (2006)] will be analyzed and compared to 40-yr European Centre for Medium-Range Weather Forecasts

(ECMWF) Re-Analysis (ERA-40) data. The effect of stratospheric dynamics on tropopause height and lower stratospheric static stability will be further investigated using offline radiative transfer calculations. Concerning the static stability structure around the tropopause and in the lower stratosphere, it will prove insightful to assess the vertical structure of the residual circulation around the tropopause. In particular, the midlatitudinal residual circulation undergoes structural changes around the tropopause. It will be shown in the present study that the corresponding vertical gradient in residual vertical velocities around the tropopause represents a positive forcing of static stability that represents a possible cause of the TIL, particularly in midlatitudes.

Section 2 describes the tools and discusses the tropopause definition used. Section 3 analyzes terms due to the residual circulation in the heat and static stability budgets. Sections 4 and 5 study the effect of stratospheric dynamics, in particular the stratospheric residual circulation, on tropopause height and lower stratospheric static stability. Finally, section 6 summarizes the main results.

2. Tools and tropopause definition

The main tools in this study are the Canadian Middle Atmosphere Mode (CMAM) simulations, complemented by results using ERA-40 (Uppala et al. 2005). CMAM represents a comprehensive chemistry–climate model (Beagley et al. 1997; Scinocca et al. 2008). The configuration used here corresponds to T47 spectral horizontal resolution and 71 vertical levels that extend up to ~100 km altitude. Around the tropopause the vertical resolution amounts to about 1 km. A 3-yr integration identical to the one used in Gettelman and Birner (2007) after spinup is used (year-to-year variability is small given that interannual variability of the prescribed sea surface temperature is not allowed). For reference, ERA-40 has a T159 horizontal resolution and 60 levels, resulting in roughly the same vertical resolution around the tropopause as CMAM. Son and Polvani (2007) found that the TIL in their simple GCM simulations depends on horizontal resolution. One would therefore expect ERA-40 with its more than 3 times higher horizontal resolution compared to CMAM to exhibit a much stronger TIL. However, data assimilation as incorporated in analyses products such as ERA-40 acts to smooth the temperature structure around the tropopause and thus leads to a weaker TIL compared to CMAM (Birner et al. 2006). Further, A. R. Erler and V. Wirth (2009, unpublished manuscript) recently found an aspect ratio of horizontal to vertical resolution of ~300–400 to be most appropriate to simulate near-tropopause dynamics (which is similar to the one discussed in Birner (2006)). The CMAM resolution aspect ratio near the tropopause is ~400, whereas it is ~120 for ERA-40; that is, ERA-40 may only represent well vertical structures around the tropopause corresponding to dynamical systems with horizontal scales about three times that of the model resolution.

An offline radiative scheme—the Column Radiation Model (CRM), a standalone version of the radiation model used in version 3 of the NCAR Community Climate Model (CCM3)—is employed in sections 4 and 5. A detailed description of the CCM3 radiative scheme can be found in Kiehl et al. (1996) and online (http://www.cgd.ucar.edu/cms/crm/). The CRM divides the solar spectrum into 18 discrete spectral intervals for ozone, water vapor, and carbon dioxide and uses a broadband approach in the longwave. Input profiles of water vapor and ozone are required and these are set to the CMAM seasonal mean profiles (see section 5). Carbon dioxide is assumed to be well mixed and set to a constant mixing ratio of 356 ppmv. Effects due to clouds are not considered in the present study; that is, only clear-sky radiative heating rates are computed. The diurnal cycle is switched off by calculating solar heating rates based on diurnally averaged solar zenith angles using a solar constant of 1367 W m^{-2}. Vertical levels in CRM are set exactly equal to CMAM model levels to ensure maximum consistency; however, the model top in CRM is set to 10 hPa (about 30 km).

Tropopause definition

A thermal tropopause definition is applied in this study. Conventionally, the thermal tropopause is defined as the lowest level at which the atmospheric lapse rate falls below 2 K km^{-1}, provided the average lapse rate between this level and all higher levels within 2 km remains below 2 K km^{-1} (WMO 1957). In the tropics, the cold point tropopause is often considered to be more appropriate, which essentially represents an alternative thermal tropopause using 0 K km^{-1} in place of the 2 K km^{-1} threshold. In the present study the sensitivity of tropopause height to a strongly perturbed stratosphere (several tens of kelvin in temperature) is investigated (see section 4). For such a strongly perturbed climate the somewhat arbitrary thresholds of 2 K km^{-1} for the lapse rate and 2 km for the thickness of the WMO definition cannot be expected to yield robust results. A different thermal tropopause criterion, based on the assumption that the troposphere and the stratosphere can be distinguished through their different thermal stratification, is therefore adopted here. We define the thermal tropopause as the level of maximum curvature of the temperature profile, that is, the level of

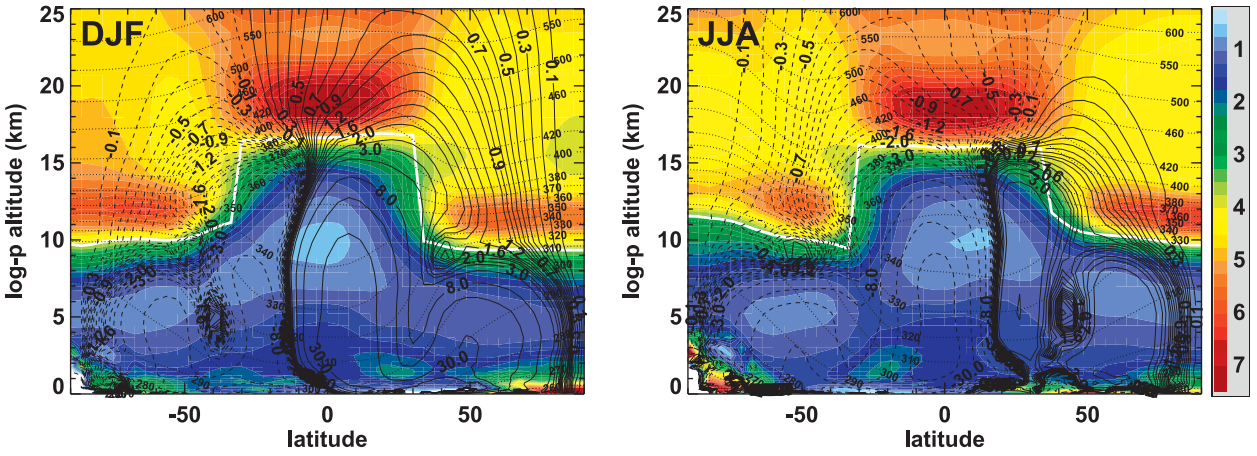

FIG. 1. Zonal mean seasonal mean buoyancy frequency squared (color shading, 10^{-4} s^{-2}) and residual streamfunction (contours, 10^2 kg m^{-1} s^{-1}, dashed lines mark negative values) for (left) DJF and (right) JJA. Streamfunction contour values are irregularly spaced at $\pm(0.1, 0.2, \ldots, 1.0, 1.2, \ldots, 2.0, 2.5, 3, 4, 8, 15, 30, 50$ kg m^{-1} s^{-1}). Thin dotted contours denote isentropes. Thick white lines mark the average position of the tropopause. Vertical axis is log-pressure altitude using a scale height of 7 km.

maximum gradient in stratification (obtained through interpolation of z onto $\partial_{zzz}T = 0$ in the neighborhood of the model level of maximum $\partial_{zz}T$). For the unperturbed climate (from CMAM or ERA-40) this maximum curvature definition yields very similar tropopause heights compared to the standard WMO definition in the extratropics and very similar tropopause heights compared to the cold point definition in the tropics. This definition is therefore also advantageous in that it represents a single appropriate tropopause definition for all latitudes. It should be noted that in this study the tropopause definition is only applied to zonal mean seasonal mean profiles; that is, robustness to, say, individual wave perturbations in the temperature profile is not critical.

3. Residual circulation forcing of heat and static stability

To gain a full picture of the effect of the residual circulation on tropopause structure and lower stratospheric static stability, we discuss the individual terms corresponding to the residual circulation in the heat and static stability budgets. An appropriate representation for this purpose is given by the TEM formulation (Andrews et al. 1987). The thermodynamic equation in classical TEM form reads:

$$\partial_t\overline{\Theta} + \overline{v}^*\partial_y\overline{\Theta} + \overline{w}^*\partial_z\overline{\Theta} = Q - \rho^{-1}\partial_z(\rho\overline{w'\Theta'} - \rho\overline{v'\Theta'}s_{\overline{\Theta}}). \quad (1)$$

This budget will be referred to as heat budget, even though, strictly speaking, it represents an entropy budget. Overbars denote zonal averages, Q denotes the diabatic heating rate of the zonal mean potential temperature (mainly due to radiation in the stratosphere), $s_{\overline{\Theta}} \equiv -\partial_y\overline{\Theta}/\partial_z\overline{\Theta}$ is the slope of the mean isentropes, and the residual velocity components are defined through

$$\overline{v}^* = -(a\rho\cos\varphi)^{-1}\partial_z\Psi^*; \quad \overline{w}^* = (a\rho\cos\varphi)^{-1}\partial_\varphi\Psi^*$$

in which

$$\Psi^* = \Psi + a\rho\cos\varphi\frac{\overline{v'\Theta'}}{\partial_z\overline{\Theta}}$$

is the residual streamfunction, with $\Psi = ag^{-1}\cos\varphi\int_{\mathrm{TOA}}^{p}v\,dp'$ the conventional (mass) streamfunction (TOA denotes top of the atmosphere). The notation here follows Juckes (2001); see also Iwasaki (1989). Note that the way the residual velocity components are computed here differs slightly from Andrews et al. (1987) mainly in that $\overline{w}$ does not enter the computation. Instead, $\overline{w}^*$ is obtained through mass balance from $\overline{v}^*$. For reference, the seasonal mean residual streamfunction Ψ^* is shown together with static stability $N^2 = g\overline{\Theta}^{-1}\partial_z\overline{\Theta}$ in Fig. 1 for boreal winter [December–February (DJF)] and boreal summer [June–August (JJA)] from CMAM. It should be noted that, unlike in Birner et al. (2006), averages of N^2 are not computed in tropopause-based coordinates here but simply in conventional pressure coordinates to facilitate comparison to the TEM streamfunction. Evidently, the resulting static stability structure around the tropopause (including the TIL signature) is not much affected in GCMs such as CMAM by the method of averaging [cf. Fig. 1 to Fig. 2(top) in Birner et al. (2006)]. Closer analysis of this somewhat surprising result suggests

that this is due to reduced variability in tropopause height in CMAM (not shown), whereas tropopause height variability in observations or meteorological analyses is sufficiently strong to blur sharp features such as the TIL in conventional coordinates.

The eddy term on the rhs of Eq. (1) represents the heat budget contribution due to cross-isentropic eddy heat fluxes. The latter can be written as $\overline{w'\Theta'}(1 - s_{\overline{\Theta}}/s_m)$, with $s_m \equiv \overline{w'\Theta'}/\overline{v'\Theta'}$ the mixing slope (cf. Held and Schneider 1999). For $s_{\overline{\Theta}} \approx s_m$ this cross-isentropic eddy heat flux contribution can be neglected, which, given that $s_{\overline{\Theta}} \ll 1$ in the region of interest here, requires that $\overline{w'\Theta'} \ll \overline{v'\Theta'}$—a good approximation in the stratosphere [see, e.g., Rosenlof (1995), in the context of the residual circulation]. The resulting heat budget then reads

$$\partial_t \overline{\Theta} \approx -\overline{v}^* \partial_y \overline{\Theta} - \overline{w}^* \partial_z \overline{\Theta} + Q. \qquad (2)$$

Results in sections 4 and 5 confirm that this approximation is appropriate in the present context. Equation (2) states that in steady state the net dynamical heating, as represented by the residual circulation terms (which include along-isentropic eddy heat flux contributions), is balanced by diabatic heating. In that sense and under the approximations used in Eq. (2), the TEM circulation represents the diabatic circulation. In fact, the TEM circulation closely resembles the isentropic-mean meridional circulation (i.e., by definition the full diabatic circulation including cross-isentropic heat fluxes) in the upper troposphere and lower stratosphere (Juckes 2001).

Under quasigeostrophic scaling, meridional advection vanishes (e.g., Andrews et al. 1987) and one obtains the simple steady-state balance $\overline{w}^* \partial_z \overline{\Theta} \approx Q$. Throughout most of the stratosphere $\partial_y \overline{\Theta} \approx 0$ and the dynamical heating in Eq. (2) should be well represented by $-\overline{w}^* \partial_z \overline{\Theta}$. In the midlatitude upper troposphere, however, $\overline{w}^* \approx 0$ (cf. Fig. 1) and dynamical heating due to vertically converging eddy heat fluxes enters the heat budget (2) through the $\overline{v}^*$ contribution (e.g., Juckes 2001). Residual circulation and eddy fluxes (of heat and momentum) are tightly coupled in that in steady state the Coriolis torque due to $\overline{v}^*$ roughly balances the Eliassen–Palm flux divergence (the potential vorticity flux in isentropic coordinates) and $\overline{w}^*$ follows from $\overline{v}^*$ through mass balance.

The individual contributions to the heat budget (2) associated with the vertical and meridional components of the residual velocity are shown for CMAM in Figs. 2a,c (DJF) and Figs. 3a,c (JJA) and their sum in Figs. 2e and 3e. Splitting up the total dynamical heating contribution into those due to the individual residual velocity components serves mainly to quantify deviations from the basic quasigeostrophic balance $\overline{w}^* \partial_z \overline{\Theta} \approx Q$, which is only expected to be accurate in the stratosphere. It is evident that the vertical ($\overline{w}^*$) contribution to the heat budget dominates the meridional contribution almost everywhere near the tropopause (consistent with quasigeostrophic scaling). Significant contributions due to the meridional residual velocity are only found in regions of elevated isentropic slopes, as expected. Negative heating (i.e., cooling) contributions due to $\overline{v}^*$ exist near the subtropical edges of the tropical tropopause, consistent with downward sloping isentropes there, that help to maintain the tropical nature of the tropopause there (note that, nevertheless, the tropopause temperature at the subtropical edge of the tropical tropopause is much higher than in the inner tropics). Warming due to $\overline{v}^*$ exists in the middle to upper midlatitude troposphere in winter (caused by vertically converging eddy heat fluxes). This warming maximizes well below the tropopause at altitudes of maximum isentropic slopes. The net dynamical tendency ($-\overline{v}^* \partial_y \overline{\Theta} - \overline{w}^* \partial_z \overline{\Theta}$) is broadly consistent with cooling in the upward and warming in the downward branches of the residual circulation (cf. Figs. 2e and 3e with Fig. 1).

Strong localized warming occurs in the subtropical upper troposphere in winter at levels that are at or just above the midlatitude and polar tropopause (~10–12 km altitude). This localized warming together with cooling further aloft represents a potentially important formation mechanism of double tropopause events, as are frequently observed in the winter subtropics (Randel et al. 2007a). The warming induced by the downwelling over the winter polar cap spans the entire column, exhibits significant vertical structure, and appears to be at a minimum around the tropopause. All of the above discussed characteristics are consistent with the full diabatic heating rate structure (not shown).

The tropopause is a feature of the vertical temperature structure. Therefore, a more clear-cut picture of the impact of large-scale dynamics as represented by the residual circulation on tropopause height arises from the contributions due to $\overline{w}^*$ and $\overline{v}^*$ to the static stability budget. Multiplying by $g/\overline{\Theta}$ and subsequently taking the vertical derivative of Eq. (2) yields an equation for static stability $\overline{N^2} = g\overline{\Theta}^{-1} \partial_z \overline{\Theta}$:

$$\partial_t \overline{N^2} \approx -\partial_z(\overline{w}^* \overline{N^2}) - g\partial_z(\overline{v}^* \overline{\Theta}^{-1} \partial_y \overline{\Theta}) + g\partial_z(\overline{\Theta}^{-1} Q). \qquad (3)$$

This equation follows exactly from the heat budget (2); the approximation sign refers to the neglect of diabatic eddy fluxes in (2). Obviously, the vertical structure of the residual circulation has the potential to impact static stability. Based on the results thus far for the heat budget and for quasigeostrophic scaling, we expect in particular the contribution due to $\overline{w}^*$ to represent a crucial factor

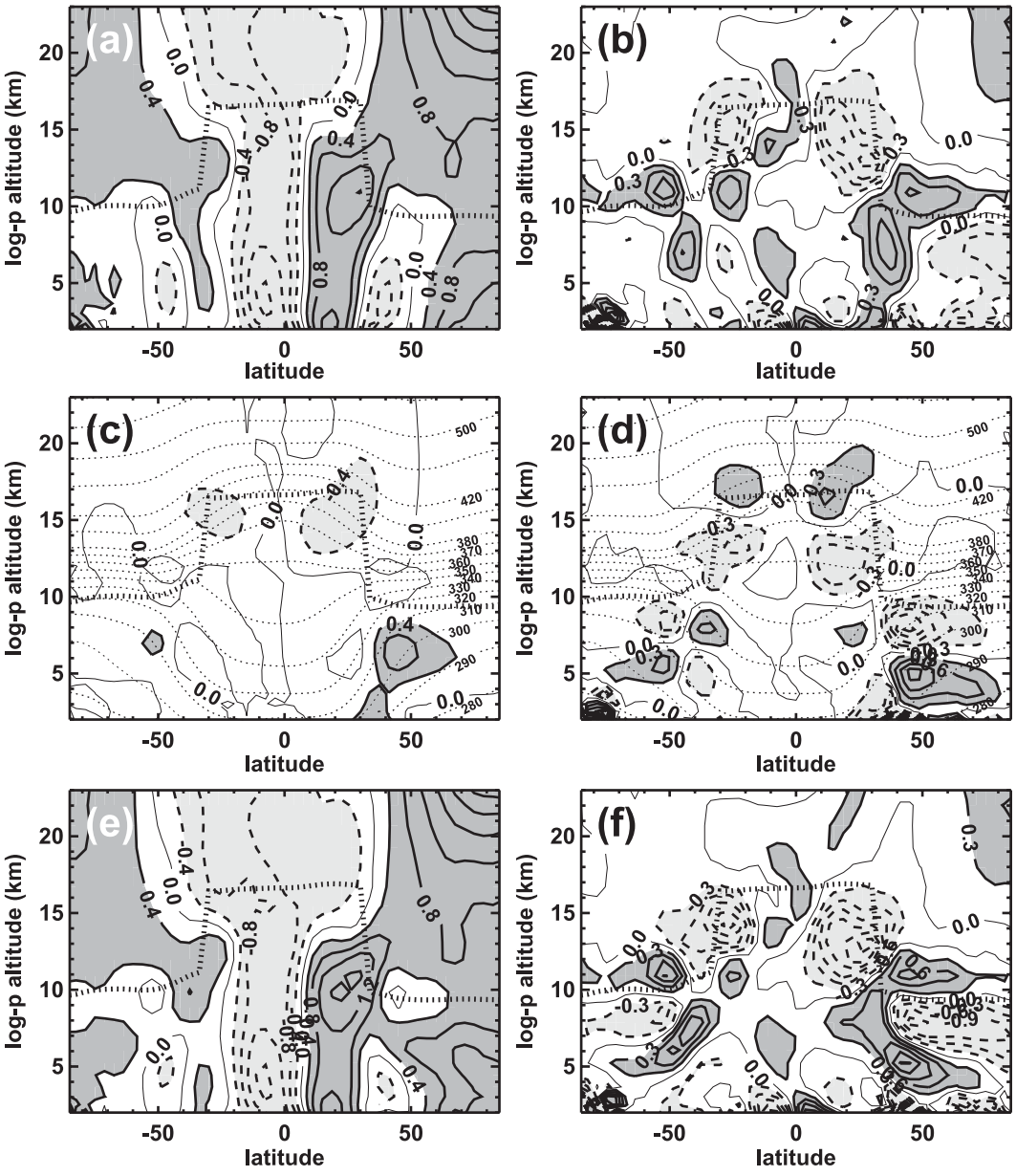

FIG. 2. (left) Dynamical heating rates as represented by the residual circulation [K day^{-1}, dark (light) shading for values greater (less) than ± 0.4 K day^{-1}] and (right) corresponding contributions to the static stability budget [10^{-5} s^{-2} day^{-1}, dark (light) shading for values greater (less) than $\pm 0.3 \times 10^{-5}$ s^{-2} day^{-1}] for DJF and CMAM. Individual terms are (a) $-\overline{w}^*\partial_z\overline{\Theta}$, (c) $-\overline{v}^*\partial_y\overline{\Theta}$, (b) $-\partial_z(\overline{w}^*\overline{N^2})$, and (d) $-g\partial_z(\overline{v}^*\overline{\Theta}^{-1}\partial_y\overline{\Theta})$ (not in sequence); (e) the sum of (a) and (c) and (f) the sum of (b) and (d). Thin dotted contours in (c) and (d) denote isentropes for reference (as in Fig. 1).

in linking the residual circulation to the static stability structure near the tropopause. In the simplest (quasigeostrophic) case one might assume a stepwise constant $\overline{N^2}$ structure and constant $\overline{w}^*$ near the tropopause. In this case the tropopause is simply advected by the residual circulation (upward in the tropics, downward in the extratropics).

Figures 2c and 2d (boreal winter, DJF) and Figs. 3c and 3d (boreal summer, JJA) show the contributions due to $\overline{w}^*$ and $\overline{v}^*$ to the static stability budget from CMAM, as well as their sum in Figs. 2f and 3f. Large negative contributions exist in the tropical and subtropical upper troposphere above ~10 km altitude (due to both $\overline{w}^*$ and $\overline{v}^*$), except for very near the equator. These negative

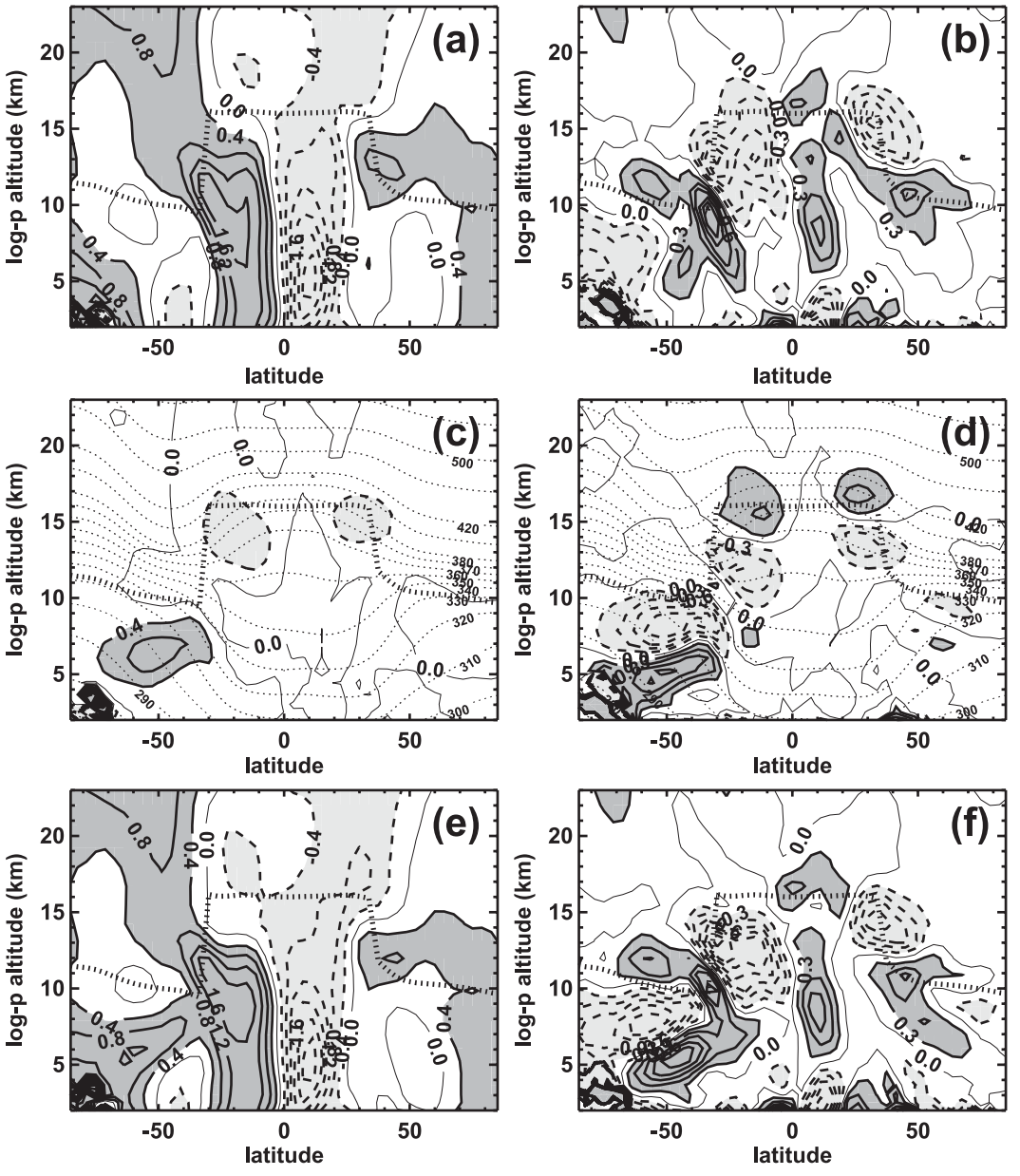

FIG. 3. As Fig. 2, but for JJA.

forcing terms in the static stability budget are consistent with an elevated tropical and subtropical tropopause. In particular, they help maintain a tropospheric lapse rate up to the level of the tropical tropopause in the subtropics. These localized forcing structures should not be confused with the overall effect due to tropospheric eddies to stabilize the bulk tropospheric lapse rate and thereby lift the tropopause. Near the equator the $\overline{w}^*$ contribution results from an incomplete compensation between a large negative forcing due to upward advection of the tropopause and a large positive forcing due to the vertical structure of $\overline{w}^*$ (not shown).

Positive forcing exists in the lowermost stratosphere at almost all latitudes, most distinctly in the winter midlatitudes (due to $\overline{w}^*$ there). This positive forcing tends to lower the extratropical tropopause but also forces a local maximum in $\overline{N^2}$ just above the extratropical tropopause, as further discussed below. On the other hand, large negative forcing in the upper extratropical troposphere (strongest in winter) is consistent with an elevated tropopause due to tropospheric eddies. This negative forcing owes to the fact that maximum warming due to tropospheric eddies occurs well below the tropopause (cf. Figs. 2c and 3c). Again, the localized negative forcing

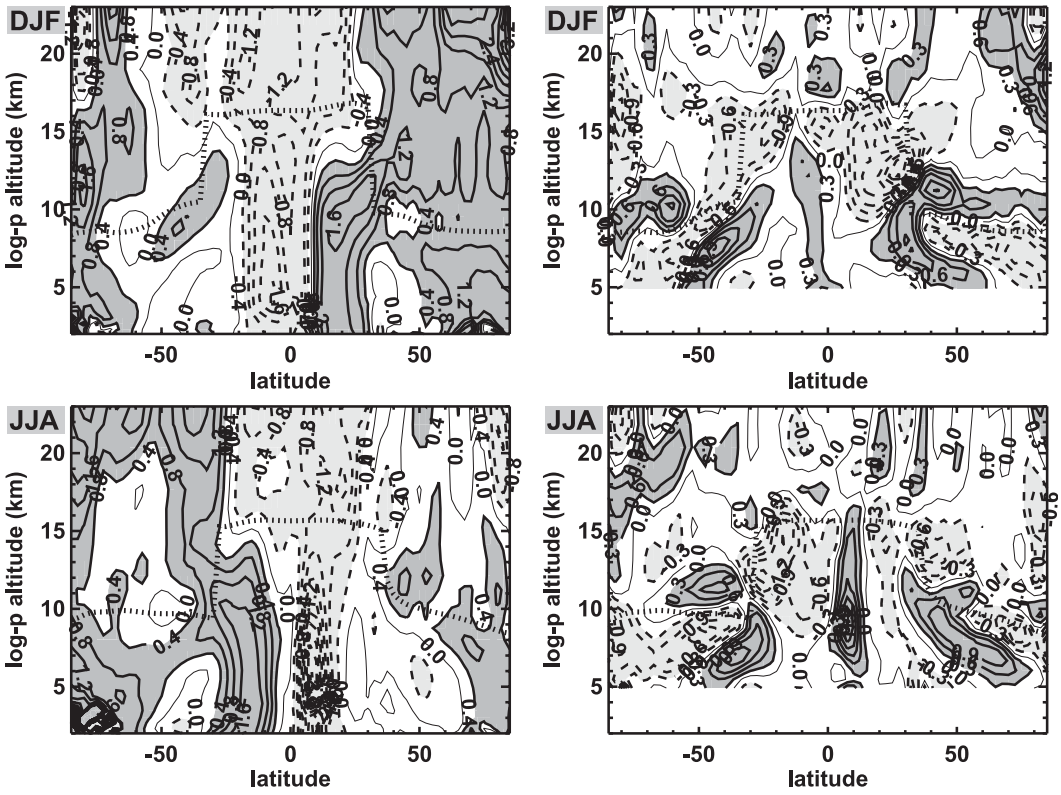

FIG. 4. As in Figs. 2 and 3e,f, but for ERA-40 (1979–2002): (top) DJF and (bottom) JJA. Forcing contributions to the static stability budget (right-hand side) become very noisy below ~5 km altitude and are not shown there.

is not in conflict with the general tendency of tropospheric eddies to stabilize the bulk tropospheric lapse rate by transporting heat poleward and upward. The net effect is a lifting of the tropopause by tropospheric eddies (cf. Egger 1995; Dell'Aquila et al. 2007) while stratospheric eddies as represented by the stratospheric circulation tend to lower the extratropical tropopause (cf. Gabriel et al. 1999; Thuburn and Craig 2000). These two opposing tendencies effectively sharpen the extratropical tropopause, especially in the winter midlatitudes. It is interesting to note that the extratropical tropopause roughly coincides with zero static stability forcing by the residual circulation (somewhat more so during DJF than during JJA). Theories for the extratropical tropopause that assume a stratosphere in radiative equilibrium (e.g., Held 1982; Schneider 2004) trivially find the tropopause to coincide with zero static stability forcing. However, in the present case this zero forcing results from the dipole structure of negative/positive forcing below/above the tropopause and as such is not due to vanishing stratospheric forcing.

Similar results concerning the residual circulation contributions to the heat and static stability budgets are obtained from ERA-40 (Fig. 4). The most notable difference between CMAM and ERA-40 exists around the tropical tropopause where ERA-40 shows a characteristic dipole structure of negative static stability forcing just below and positive static stability forcing just above the tropopause (similar to the behavior in midlatitudes). CMAM, on the other hand, shows positive static stability forcing due to the residual circulation throughout the tropical upper troposphere and lower stratosphere, even though this positive forcing appears to be enhanced in the lowermost stratosphere, as in ERA-40.

4. Effect of stratospheric dynamics on tropopause height

Stratospheric dynamics as represented by the residual circulation induces departures from local radiative equilibrium temperatures (Θ_{rad}) with temperatures colder than Θ_{rad} within the tropical upward branch and temperatures warmer than Θ_{rad} within the extratropical downward branch. To quantify this departure and the overall effect of stratospheric dynamics on tropopause structure and lower stratospheric static stability, we first use the CRM as described in section 2 to compute

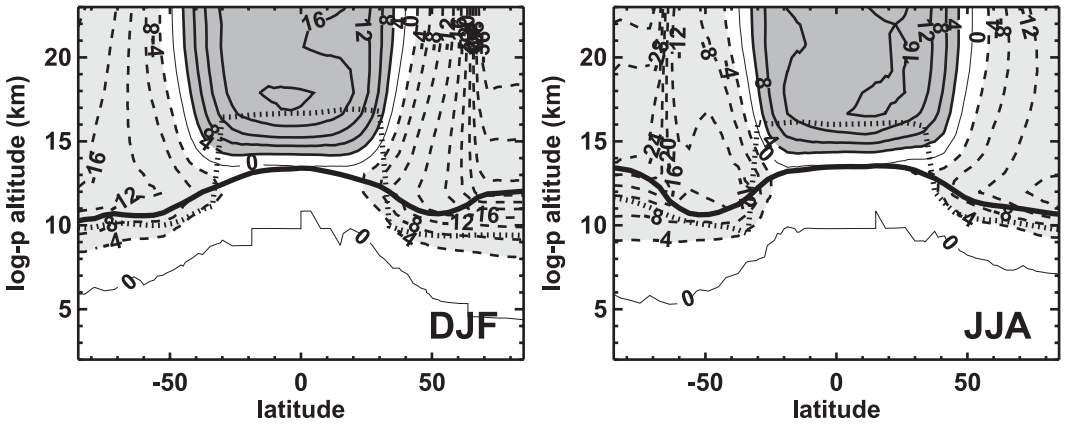

FIG. 5. Temperature difference $T_{\text{rad}}^{\text{str}} - \overline{T}_{\text{CMAM}}$ for (left) DJF and (right) JJA. Contour interval is 4 K; dashed contours correspond to negative values. Thick full lines denote the tropopause for the stratospheric radiative equilibrium state; dotted lines denote the CMAM reference tropopause.

stratospheric radiative equilibrium (SRE) solutions given the CMAM simulated seasonal mean water vapor and ozone distributions. These SRE solutions assume a given, quasi-fixed tropospheric climate that closely resembles the one simulated by CMAM (''quasi-fixed'' refers to slight necessary adjustments in the upper troposphere to prevent superadiabatic lapse rates; see appendix A for details). That is, a hypothetical climate state with a troposphere as simulated by CMAM and a stratosphere in radiative equilibrium is computed. It should be noted that the distributions of water vapor and ozone as simulated by CMAM are shaped in part by stratospheric dynamics (e.g., ozone mixing ratios in the polar winter stratosphere would be much lower without the contribution due to the Brewer–Dobson circulation). As such, the SRE as defined here still includes the indirect effect of stratospheric dynamics due to the altered distributions of water vapor and ozone.

Figure 5 shows the temperature difference between CMAM and the SRE solution for DJF and JJA. As expected the SRE solution exhibits a warmer tropical stratosphere and a colder extratropical stratosphere, consistent with radiative warming due to the upward branch and radiative cooling due to the downward branch of the residual circulation. This temperature difference is larger during DJF than during JJA, reflecting the seasonal contrast in the strength of the circulation. Tropical temperature profiles of the SRE solution hardly show a difference between DJF and JJA (not shown). It is furthermore interesting to note that the largest temperature difference in the tropics exists just above the tropopause, consistent with a maximized radiative time scale there (Randel et al. 2002). The zero lines in Fig. 5 in the stratosphere roughly coincide with the zero heating lines due to the residual circulation in Figs. 2e and 3e, confirming that the major balance in the stratospheric heat budget exists between circulation-induced forcing and radiation.

The tropopause of the SRE solution is located much lower in the tropics and somewhat higher in the extratropics compared to CMAM. That is, the difference between the tropical and extratropical tropopause is much reduced in the SRE solution compared to CMAM with the tropics playing the dominant role in the change of the equator-to-pole contrast in tropopause height. Apparently, stratospheric dynamics provide a leading order contribution to the equator-to-pole contrast in tropopause height, consistent with Kirk-Davidoff and Lindzen (2000).

In the tropics the SRE tropopause is located just above the top of convection at ~12 km altitude (cf. Gettelman and Birner 2007). This suggests that the thermal properties of the layer between the top of convection and the tropical tropopause—the tropical tropopause layer—are predominantly set by the stratospheric residual circulation on average (cf. Highwood and Hoskins 1998), but a more detailed investigation is required to confirm this. In contrast, Thuburn and Craig (2002) find a well-separated tropical tropopause from the top of convection in their radiative–convective equilibrium solution (i.e., without any tropical upwelling-induced cooling). Reasons for this discrepancy are presently unclear but are possibly related to the way the troposphere is treated [i.e., convective adjustment to constant lapse rate in Thuburn and Craig (2002), the CMAM height-dependent lapse rate here].

Further, the polar tropopause during winter is elevated compared to midlatitudes in the SRE solution, especially in southern polar winter where the tropopause attains altitudes as high as in the tropics. This is

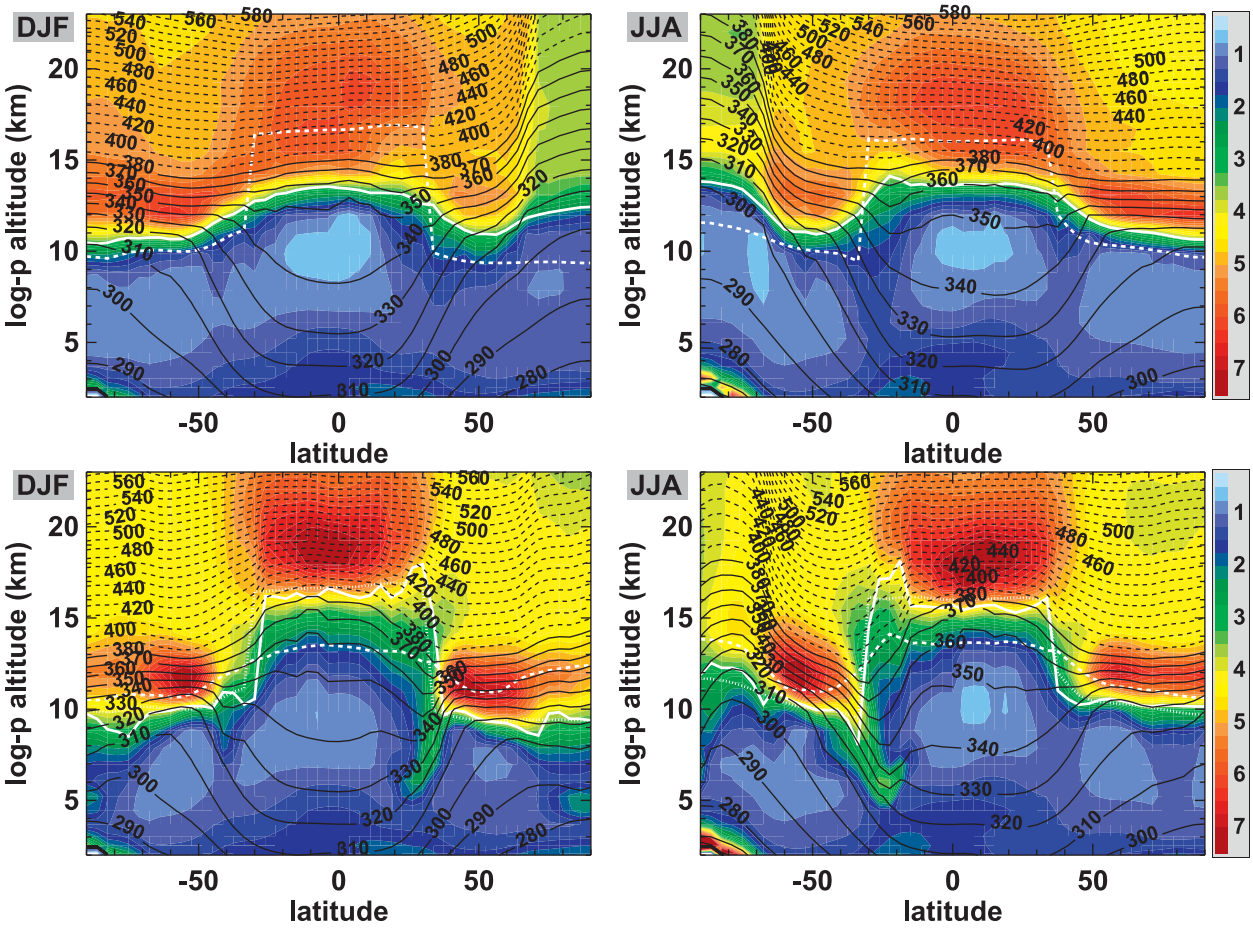

FIG. 6. (top) Stratospheric radiative equilibrium solutions of $\overline{N^2}$ (color shading, 10^{-4} s^{-2}), $\overline{\Theta}$ (contours, K), and tropopause height (white full line), as obtained by constraining the troposphere to CMAM's solution. All dynamical heating contributions have been set to zero above the tropopause. Dashed white line marks CMAM's tropopause height. (bottom) As in top, but for stratospheric radiation–circulation solutions (equilibrium between radiation and circulation-induced dynamical heating).

consistent with the largest differences in static stability between the SRE solution and CMAM in polar winter (Fig. 6, top), when the missing heating in the SRE solution due to solar radiation and dynamics causes temperatures to continue to decrease throughout the stratosphere (see also Zängl 2002). A strong vertical gradient in static stability, that is, a tropopause, still exists but is located much higher than in CMAM. Note that by definition the tropopause, as defined in this study, in general coincides with the level of maximum gradient in $\overline{N^2}$ (maximum curvature in temperature), which very clearly separates layers of different stratification (the troposphere and the stratosphere). In the polar regions during winter the lower stratospheric stratification in the SRE solution drops below the threshold used in the conventional (WMO) thermal tropopause definition such that the WMO definition would yield tropopause heights several kilometers higher than shown in Figs. 5 and 6 (top).

The difference in tropopause height between CMAM and the SRE solution is further quantified in Fig. 7 (solid lines). Throughout the tropics the introduction of stratospheric dynamics causes an elevation of the tropopause by about 3–4 km compared to a stratosphere in radiative equilibrium. In the extratropics the change in tropopause height is not as dramatic but still ranges between 1 and 2 km, with somewhat larger values during winter, especially in the polar regions as discussed above. Overall, stratospheric dynamics roughly lead to a more than doubled equator-to-pole contrast in tropopause height (~3 km in the SRE solution compared to ~8 km in CMAM or ERA-40).

In the heat budget (2) it was assumed that most of the stratospheric dynamical heating is due to the residual circulation by neglecting cross-isentropic eddy heat flux contributions. To test this assumption, equilibrium solutions of Eq. (2) have been obtained for the stratosphere using CMAM's residual velocities and clear-sky

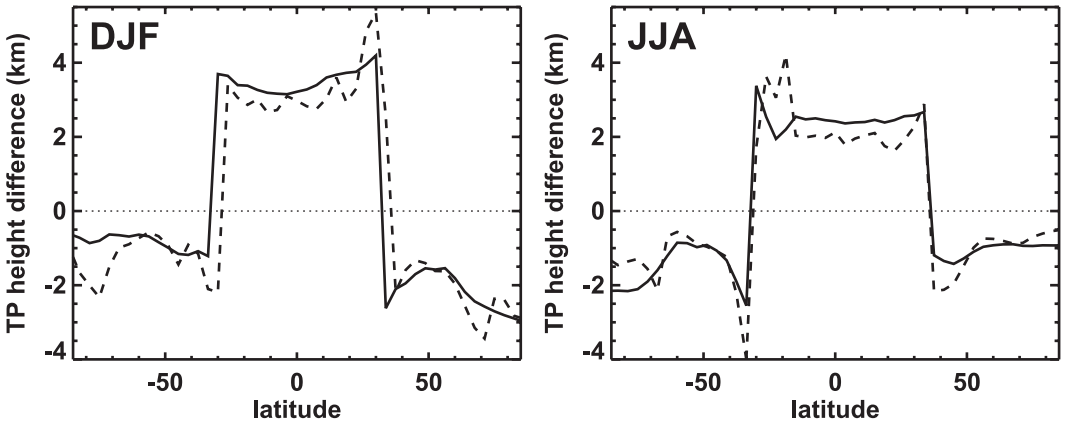

FIG. 7. Tropopause height difference between CMAM and the stratospheric radiative equilibrium (solid lines) and between the circulation–radiation solution and the stratospheric radiative equilibrium (dashed lines): (left) DJF and (right) JJA.

radiation, as before from the CRM, in place of Q. As in the case of the SRE solution, the troposphere was quasi fixed in these stratospheric circulation–radiation solutions (hereafter SCR solutions). The dashed lines in Fig. 7 show the difference in tropopause height between the SCR solution and the SRE solution, which qualitatively resembles the difference between CMAM and the SRE solution (full lines). Large differences generally occur in the subtropics where the meridional gradient in tropopause height is large. Further, the circulation-induced elevation of the tropical tropopause falls short of the total amount in CMAM, which includes all dynamical (and diabatic) contributions. Larger discrepancies also occur near the South Pole. Nevertheless, overall the SCR solution captures the main modification of tropopause height [and static stability; see Fig. 6 (bottom) and next section] that comes about due to stratospheric dynamics.

5. Effect of stratospheric dynamics on lower stratospheric static stability

a. General structure

Figure 6 (top) shows the static stability structure of the SRE solution. The tropical stratosphere in the SRE solution exhibits smaller static stability compared to CMAM; in particular, the lower stratospheric static stability maximum (corresponding to the tropical TIL) is not as pronounced in the SRE solution, suggesting that dynamics play a significant role in causing this maximum. The midlatitudinal static stability maximum (TIL) almost disappears in the SRE solution during winter, especially in the Northern Hemisphere. The summer TIL in the extratropics, on the other hand, remains intact compared to CMAM, suggesting that radiation plays a dominant role in the formation of the TIL there. Lower stratospheric static stability is generally larger in the extratropics of the SRE solution compared to CMAM (outside the winter polar regions).

Figure 6 (bottom) shows the static stability structure of the SCR solution, which qualitatively resembles the CMAM static stability structure. The strongest difference from the SRE solution is the existence of a strong static stability maximum (TIL) in midlatitudes during winter in the SCR solution. This suggests that stratospheric dynamics, as represented by the residual circulation, represents the main cause of the TIL in midlatitudes during winter, at least in CMAM. Closer inspection of the strength of the static stability maximum in the SCR solution reveals that it is stronger than in CMAM. This is largely due to missing vertical diffusion (both eddy and numerical) in the SCR solution, which plays an important role in limiting static stability around the tropopause in CMAM (not shown). The tropical TIL is much more pronounced in the SCR solution than in the SRE solution, suggesting that the residual circulation represents a main forcing for the TIL there as well.

b. Extratropical tropopause inversion layer

As discussed above, the residual circulation represents a strong positive forcing of static stability, in particular in the lowermost extratropical stratosphere. We will therefore now discuss this feature in more detail.

1) VERTICAL STRUCTURE OF RESIDUAL CIRCULATION

The residual circulation near the extratropical tropopause in CMAM exhibits a characteristic vertical structure (Fig. 1): in particular, residual vertical velocities

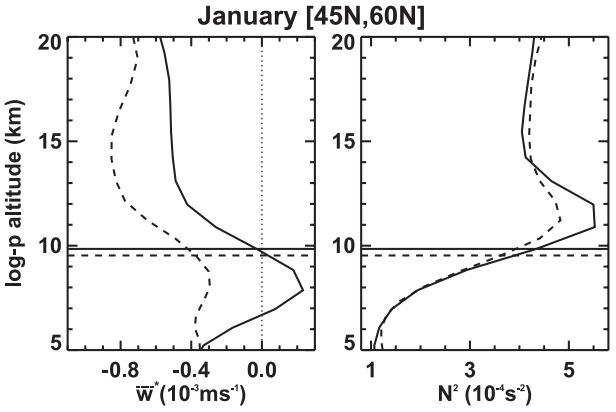

FIG. 8. (left) Residual vertical velocity and (right) buoyancy frequency squared as a function of altitude for January averaged over the latitude band 45°–60°N. Results from CMAM (solid lines) and ERA-40 (dashed lines, years 1979–2002) are shown. Horizontal lines mark the average location of the tropopause. The dotted vertical line in the left panel marks $\overline{w}^* = 0$.

undergo a rather strong transition from near-zero values in the extratropical upper troposphere to negative values in the extratropical lower stratosphere. The above behavior is much more pronounced in winter than in summer (cf. Fig. 1), reflecting mainly the seasonal contrast in the stratospheric part of the residual circulation.

As discussed in section 3, the dynamical static stability forcing is dominated by the contribution due to $\overline{w}^*$ throughout the lowermost stratosphere, consistent with quasigeostrophic scaling. For the purpose of discussing the TIL signature it therefore seems appropriate to approximate the static stability budget at the level of maximum $\overline{N^2}$ (hereafter $\overline{N^2}_{\max}$) as

$$\partial_t \overline{N^2}_{\max} \approx -\partial_z(\overline{w}^*\overline{N^2})|_{\max} + g\partial_z(\overline{\Theta}^{-1}Q)|_{\max} = -\overline{N^2}_{\max}\partial_z\overline{w}^*|_{\max} + g\partial_z(\overline{\Theta}^{-1}Q)|_{\max}, \quad (4)$$

where the last expression takes into account that $\partial_z\overline{N^2}|_{\max} = 0$ (one might also more generally interpret this expression as the tendency of an initial value problem starting with constant stratospheric $\overline{N^2}$). In this case $-\overline{N^2}\partial_z\overline{w}^*$ is the only dynamical static stability forcing term. Note that this forcing term has been discussed previously in a slightly different context of the ageostrophic circulation in upper-level balanced disturbances (Wirth 2004; Wirth and Szabo 2007). For $\overline{N^2} > 0$ (stable stratification) $\partial_z\overline{w}^* < 0$ leads to positive forcing of $\overline{N^2}$, whereas $\partial_z\overline{w}^* > 0$ leads to negative forcing of $\overline{N^2}$. This forcing for given $\partial_z\overline{w}^*$ is amplified in regions where $\overline{N^2}$ is large (the stratosphere). In the midlatitudinal upper troposphere $\overline{w}^* \approx 0$, whereas $\overline{w}^* < 0$ in the midlatitudinal stratosphere; therefore, $\partial_z\overline{w}^* < 0$ near TIL altitudes. Figure 8 demonstrates that the strongest (negative) vertical gradient in $\overline{w}^*$ in midlatitudes during winter occurs in the altitude range of maximum $\overline{N^2}$ for both CMAM and ERA-40.

2) ANNUAL CYCLE

The strength of the stratospheric residual circulation varies strongly with season. The strength of the dynamical forcing term $-\overline{N^2}_{\max}\partial_z\overline{w}^*|_{\max}$ in Eq. (4) should therefore also exhibit a pronounced seasonal cycle. Figure 9 displays the annual cycle of $-\partial_z\overline{w}^*|_{\max}$ at northern midlatitudes together with the annual cycles of the maximum of the zonal mean N^2 (i.e., $\overline{N^2}_{\max}$) and the zonal mean of (instantaneous) maximum N^2 for CMAM and ERA-40. The forcing, approximately $-\partial_z\overline{w}^*|_{\max}$, maximizes in December (CMAM) and January (ERA-40), whereas $\overline{N^2}_{\max}$ maximizes 2–4 months later in March–April (CMAM) and March (ERA-40). This delay between the annual cycles of $-\partial_z\overline{w}^*|_{\max}$ and $\overline{N^2}_{\max}$ agrees qualitatively with the deduced time scale of ≈70 days at maximum forcing [$\max(-\partial_z\overline{w}^*|_{\max}) \approx 0.014$ day^{-1} ≈ (70 days)$^{-1}$]. The 2–4-month offset with $-\partial_z\overline{w}^*|_{\max}$ leading $\overline{N^2}_{\max}$ holds roughly throughout the course of the year. Forcing magnitudes are similar in CMAM and ERA-40. Averages of instantaneous maximum N^2 follow a somewhat different annual cycle from $\overline{N^2}_{\max}$ in the case of ERA-40 (cf. dashed and dotted lines in Fig. 9, right), indicating that tropopause variability is sufficiently large to affect averaging for ERA-40 [cf. also the recent observational analysis of the TIL annual cycle by Grise et al. (2010)].

The same relationship between the annual cycles of $-\partial_z\overline{w}^*|_{\max}$ and $\overline{N^2}_{\max}$ does not hold at polar latitudes (Fig. 10) where $\overline{N^2}_{\max}$ maximizes during summer, in contrast to the behavior at midlatitudes: $-\partial_z\overline{w}^*|_{\max}$ still provides a positive forcing during winter but is less than half as strong as in midlatitudes. Furthermore, $-\partial_z\overline{w}^*|_{\max}$ is around zero (negative for CMAM) during summer when $\overline{N^2}_{\max}$ is largest. That is, other processes such as radiation (Randel et al. 2007b; Kunz et al. 2009) must be responsible for the TIL in the polar regions, especially in summer (see previous subsection). It therefore appears that the TIL at midlatitudes in winter and the TIL at polar latitudes in summer represent two distinct phenomena.

3) SIMPLE ARGUMENTS

In the stratosphere the diabatic heating Q tends to be dominated by radiative heating, which is often approximated by simple Newtonian damping:

$$Q \approx Q_{\text{rad}} \approx \tau_{\text{rad}}^{-1}(\Theta_{\text{rad}} - \overline{\Theta}), \quad (5)$$

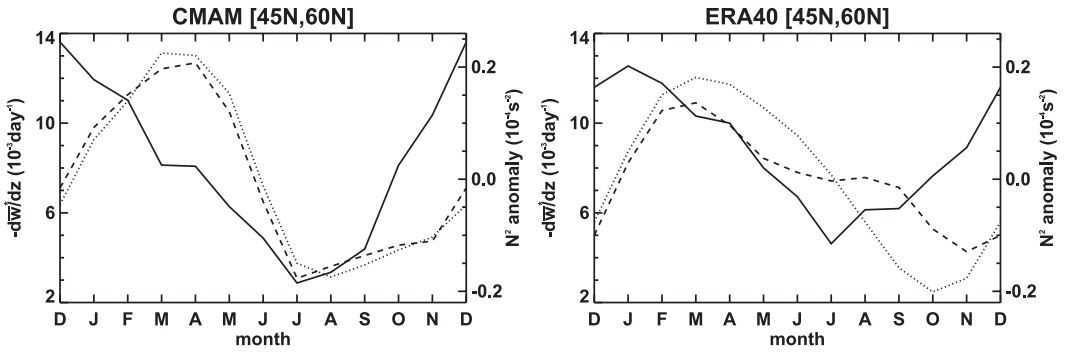

FIG. 9. Annual cycles of residual vertical velocity gradient $\partial_z \overline{w}^*$ (solid) and buoyancy frequency squared (dashed) evaluated at the level of maximum zonal mean N^2 and averaged over the latitude band 45°–60°N for (left) CMAM and (right) ERA-40 (1979–2001). Dotted lines refer to the monthly climatologies of instantaneous maximum values of N^2. All N^2 curves are defined relative to their annual mean. The annual means of maximum zonal mean N^2 are 5.5 and 4.8×10^{-4} s^{-2} for CMAM and ERA-40, respectively. The annual means of instantaneous maximum N^2 are 6.2 and 5.6×10^{-4} s^{-2} for CMAM and ERA-40, respectively. Note that $\partial_z \overline{w}^*$ maximizes about 2–3 months prior to N^2.

where $\tau_{\rm rad}$ represents the radiative damping time scale (typically ~30–60 days) and $\Theta_{\rm rad}$ represents the (hypothetical) radiative equilibrium potential temperature. The corresponding diabatic forcing term in the static stability budget (3) then becomes

$$g\partial_z(\overline{\Theta}^{-1}Q_{\rm rad}) \approx \frac{\Theta_{\rm rad}}{\overline{\Theta}}\tau_{\rm rad}^{-1}(N^2_{\rm rad} - \overline{N^2}) + g\left(\frac{\Theta_{\rm rad}}{\overline{\Theta}} - 1\right)\partial_z\tau_{\rm rad}^{-1} \tag{6}$$

$$= \frac{\Theta_{\rm rad}}{\overline{\Theta}}\tau_{\rm rad}^{-1}(N^2_{\rm rad} - \overline{N^2}) - \frac{g}{\overline{\Theta}}Q_{\rm rad}\tau_{\rm rad}^{-1}\partial_z\tau_{\rm rad} \tag{7}$$

[the approximation sign refers to the approximation sign in Eq. (5)].

Assuming $(\overline{\Theta} - \Theta_{\rm rad})/\Theta_{\rm rad} \ll 1$ and $\tau_{\rm rad}$ independent of altitude yields the simple radiative static stability forcing $\tau_{\rm rad}^{-1}(N^2_{\rm rad} - \overline{N^2}_{\rm max})$ at the level of maximum $\overline{N^2}$. Equation (4) then becomes

$$\partial_t \overline{N^2}_{\rm max} \approx -\partial_z \overline{w}^*|_{\rm max}\overline{N^2}_{\rm max} + \tau_{\rm rad}^{-1}(N^2_{\rm rad} - \overline{N^2}_{\rm max}) \tag{8}$$

$$= -(\tau_{\rm rad}^{-1} - \tau_{\rm dyn}^{-1})\overline{N^2}_{\rm max} + \tau_{\rm rad}^{-1}N^2_{\rm rad}, \tag{9}$$

with the shorthand notation $\tau_{\rm dyn} = (-\partial_z \overline{w}^*|_{\rm max})^{-1}$ ($\tau_{\rm dyn}$ has units of time but, strictly speaking, is not equal to the dynamical time scale of the problem that in steady-state balance would equal $\tau_{\rm rad}$). For constant $\tau_{\rm dyn}$ (say, corresponding to the annual mean value) this yields a time scale of adjustment to equilibrium of $\tau_{\rm equ} = \tau_{\rm rad}(1 - \tau_{\rm rad}/\tau_{\rm dyn})^{-1}$ and an equilibrium solution of

$$\overline{N^2}_{\rm max} = \frac{1}{1 - \tau_{\rm rad}/\tau_{\rm dyn}}N^2_{\rm rad}. \tag{10}$$

In the annual mean $\tau_{\rm dyn} \sim 120$ days for CMAM (northern midlatitudes, see Fig. 9); that is, $\tau_{\rm dyn}/\tau_{\rm rad} \sim 2$–4 using $\tau_{\rm rad} \sim 30$–60 days. In this case an equilibration time scale of $\tau_{\rm equ}/\tau_{\rm rad} \sim 4/3 - 2$ results and $\overline{N^2}_{\rm max}/N^2_{\rm rad} \sim 4/3 - 2$. These values for $\overline{N^2}_{\rm max}$ are consistent with the CMAM annual mean $\overline{N^2}_{\rm max}$, given $N^2_{\rm rad} \sim 4 \times 10^{-4}$ s^{-2}. Interestingly, the annual mean forcing in ERA-40 is somewhat larger (smaller $\tau_{\rm dyn}$) than in CMAM, which would lead to a larger $\overline{N^2}_{\rm max}$, whereas the actual $\overline{N^2}_{\rm max}$ value is smaller in ERA-40 than in CMAM. This might be related to issues with the data assimilation in ERA-40 as elaborated in section 2.

For northern midlatitudinal winter (DJF) $\tau_{\rm dyn} \sim 80$ days; that is, $\tau_{\rm dyn}/\tau_{\rm rad} \sim 4/3 - 8/3$ (again using $\tau_{\rm rad} \sim 30$–60 days). This yields a range for the equilibration time scale of $\tau_{\rm equ} \sim 50$–240 days, whose lower half is consistent with the 60–120-day offset of $\overline{N^2}_{\rm max}$ compared to the forcing, approximately $-\partial_z \overline{w}^*|_{\rm max}$ (Fig. 9). In this case, $\overline{N^2}_{\rm max} \sim (6.4\text{–}16) \times 10^{-4}$ s^{-2} (again using $N^2_{\rm rad} \sim 4 \times 10^{-4}$ s^{-2}), which fits instantaneous $\overline{N^2}_{\rm max}$ values at its lower boundary (~6.4×10^{-4} s^{-2} during March–April) but tends to predict too large $\overline{N^2}_{\rm max}$ values. It should be emphasized that Eq. (8) represents an approximation of the full static stability budget. In the full CMAM simulation other processes impact the value $\overline{N^2}_{\rm max}$, for example, vertical diffusion, which tends to reduce $\overline{N^2}_{\rm max}$). Very similar relationships arise for ERA-40.

In the polar regions radiation seems to represent the dominant cause of the TIL, especially during summer (cf. Figs. 1 and 6). During winter dynamical forcing might play a role: $\tau_{\rm dyn} \sim 200$ days; that is,

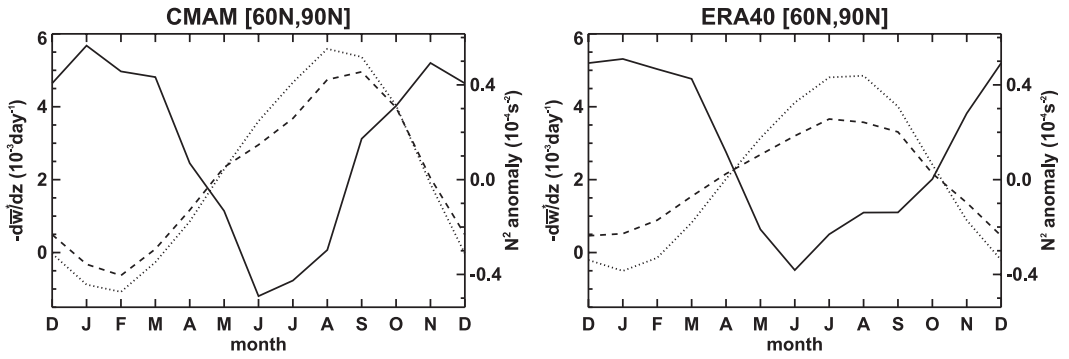

FIG. 10. As in Fig. 9, but for the latitude band 60°–90°N. The annual means of maximum zonal mean N^2 are 6.0 and 4.9×10^{-4} s^{-2} for CMAM and ERA-40, respectively. The annual means of instantaneous maximum N^2 are 6.8 and 5.8×10^{-4} s^{-2} for CMAM and ERA-40, respectively.

$\tau_{dyn}/\tau_{rad} \sim 10/3 - 20/3$. Using $N^2_{rad} \sim 4 \times 10^{-4}$ s^{-2} as before yields $\overline{N^2_{max}} \sim (4.7-5.7) \times 10^{-4}$ s^{-2}, which fits the CMAM winter values of $\overline{N^2_{max}} \approx 5.6 \times 10^{-4}$ s^{-2}. However, N^2_{rad} should in fact be set to a lower value during polar winter, leading to only a partial dynamical explanation of $\overline{N^2_{max}}$.

The SCR solution discussed above and shown in Fig. 6 represents an equilibrium between the forcing due to the residual circulation and clear-sky radiation. A similar solution can also be obtained by replacing the radiative forcing in Eq. (2) by Newtonian damping, Eq. (5), using a given radiative time scale τ_{rad} and (hypothetical) radiative equilibrium distribution Θ_{rad}. Figure 11 (top) shows such hypothetical Θ_{rad} distributions along with corresponding N^2_{rad} distributions for DJF and JJA (see appendix B for technical details of the specified radiative equilibrium distributions as well as τ_{rad}). Evidently, and by construction, this hypothetical radiative equilibrium distribution does not contain a TIL.

Initialized with the radiative equilibrium distribution $\overline{\Theta}(t = 0, \varphi, z) = \Theta_{rad}(\varphi, z)$, Eq. (2) is integrated forward in time applying the Newtonian damping approximation (5) until equilibration ($\gtrsim$100 days). Figure 11 (bottom) shows the resulting distributions of $\overline{\Theta}$ and $\overline{N^2}$ for DJF and JJA. A TIL is formed most strongly at midlatitudes during winter. A weaker TIL also exists during summer in midlatitudes, whereas virtually no TIL is simulated in the polar regions—in particular, the strong TIL in polar summer is basically absent. This confirms the results obtained from the SCR solution in a strongly idealized framework. It is also noteworthy that the circulation shows a strong tendency to form a double tropopause structure in the subtropics.

6. Summary and discussion

The effect of large-scale dynamics as represented by the residual mean meridional circulation in a TEM sense, in particular its stratospheric part, on lower stratospheric static stability and tropopause structure has been investigated using a chemistry–climate model, reanalysis data, and simple idealized modeling. Upwelling in the tropics induces cooling and therefore lifts the tropopause, whereas downwelling in the extratropics induces warming that lowers the tropopause (cf. Thuburn and Craig 2000; Wong and Wang 2003). These circulation-induced changes in tropopause height are consistent with corresponding forcing contributions in the static stability budget that constitute a strong localized positive forcing of static stability just above the tropopause, most pronounced in the winter midlatitudes. This strong positive forcing due to the stratospheric residual circulation (i.e., due to stratospheric eddies) causes a local maximum in static stability just above the tropopause, especially in the winter midlatitudes, corresponding to the so-called tropopause inversion layer (TIL). Strong negative static stability forcing due to the residual circulation is diagnosed in the extratropical upper troposphere (i.e., due to tropospheric eddies). This negative forcing is consistent with the tendency of tropospheric eddies to lift the tropopause, opposing the tendency due to the positive lower stratospheric forcing. The resulting dipole forcing structure effectively sharpens the extratropical tropopause. In fact, the extratropical tropopause roughly coincides with zero forcing of static stability due to the residual circulation.

Strong negative static stability forcing due to the residual circulation is also found in the subtropical upper troposphere in a region of strong meridional temperature and static stability gradients, which helps to maintain low static stability and a high and cold tropopause there. Near the subtropical edge of the tropical tropopause this negative static stability forcing overlies positive forcing due to the circulation around the level of the extratropical tropopause. This favors the frequent formation of a double tropopause in the subtropics, especially during winter.

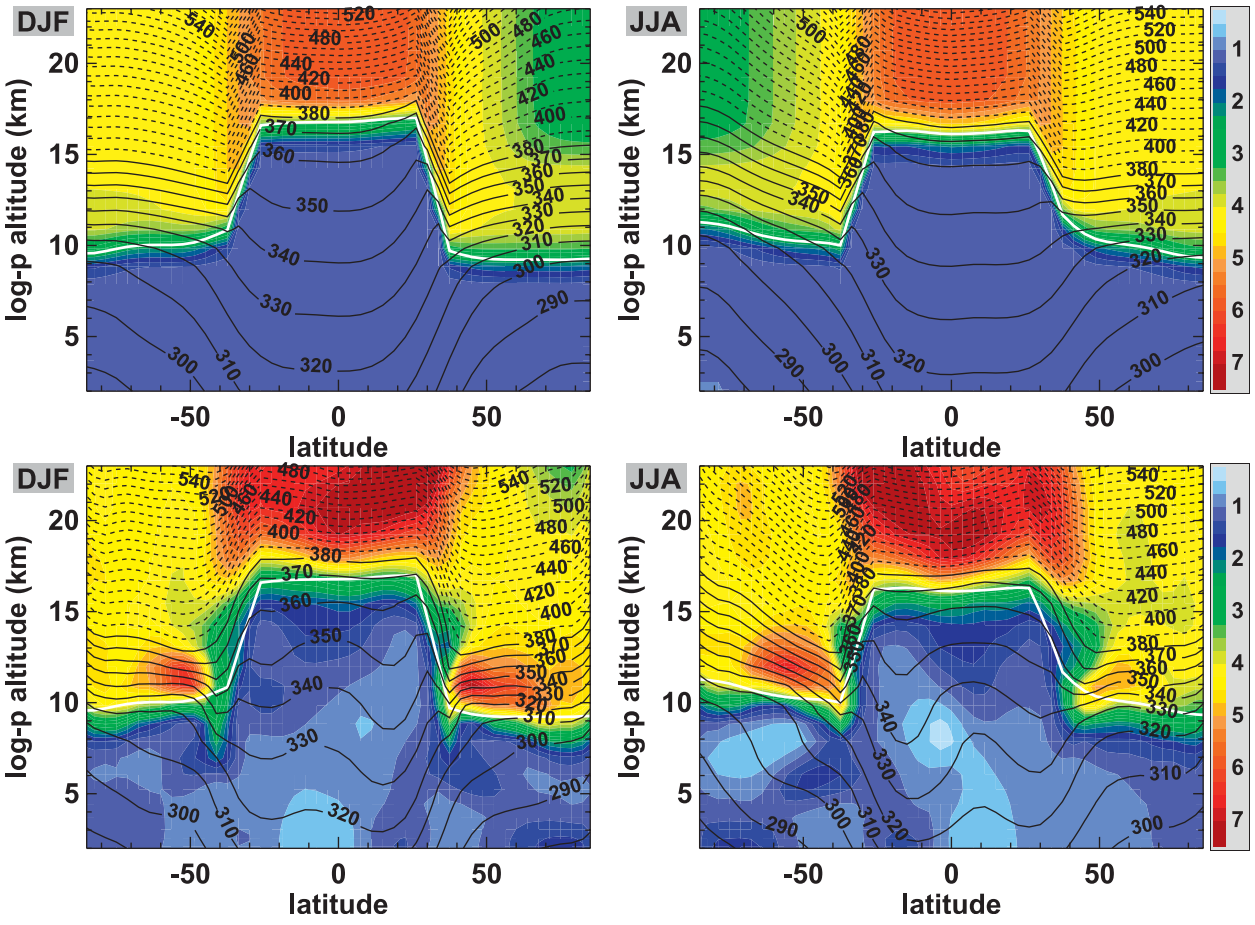

FIG. 11. (top) Assumed hypothetical radiative equilibrium static stability (N^2_{rad}, color shading, 10^{-4} s^{-2}) and potential temperature (Θ_{rad}, contours, K) distribution (see text), and (bottom) solution of circulation-induced heating with Newtonian damping, for (left) DJF and (right) JJA. White line marks tropopause.

The results summarized above rely on a TEM perspective that assumes cross-isentropic (diabatic) eddy heat fluxes to be negligible in the heat budget; see discussion around Eq. (2). This allows the residual circulation to be interpreted as the diabatic circulation; that is, the dynamical heating rates are given by the advection of $\overline{\Theta}$ by the residual circulation. In the stratosphere this is generally accepted to represent a good approximation (e.g., Rosenlof 1995). In the troposphere, however, diabatic effects, such as related to latent heat release, can often not be neglected, as remarked by Held and Schneider (1999). Nevertheless, the TEM circulation approximates the diabatic (isentropic mean) circulation well in the upper troposphere and lower stratosphere (cf. Juckes 2001), that is, in the region of interest in the present study. A comparison between the residual-circulation-induced heating rate (e.g., Fig. 2e) with the full diabatic heating rate reveals some quantitative differences between the two in the upper troposphere and at the tropical tropopause (not shown); however, the overall qualitative structures, as discussed in section 3, agree very well. The dynamical forcing of the thermal structure around the tropopause as represented by the residual circulation is therefore consistent with the full dynamical forcing including diabatic effects in the upper troposphere.

Theories for the height of the tropopause conventionally assume a stratosphere in (local) radiative equilibrium (e.g., Schneider 2007 and references therein). Different tropical and extratropical tropopause heights result from different tropospheric lapse rates and surface temperatures in these theories. To test the impact of stratospheric dynamics on tropopause height, a (hypothetical) stratospheric radiative equilibrium (SRE) solution has been obtained using the CCM distributions of water vapor and ozone and by constraining the troposphere to remain quasi fixed to the CCM troposphere (i.e., a realistic tropospheric lapse rate structure is prescribed, in contrast to conventional radiative–convective equilibrium studies, which typically assume a constant

tropospheric lapse rate, that may depend on latitude). The tropopause in this SRE solution is strongly reduced in the tropics (by 3–4 km). The cold point tropopause and the top of convection do not appear to be well separated in the tropical SRE solution (i.e., a TTL does not exist), in contrast to the results in Thuburn and Craig (2002) based on radiative–convective equilibrium solutions that assume a constant tropospheric lapse rate. The reasons for this discrepancy are currently unclear and deserve further investigation. The extratropical tropopause in the SRE solution is located higher than in the CCM (by 1–2 km, around 11–12 km consistent with radiative–convective equilibrium estimates; e.g., Fig. 1b in Thuburn and Craig 2000), resulting in a strongly reduced equator-to-pole contrast (less than half of that of the CCM). Kirk-Davidoff and Lindzen (2000) obtained a similarly strong influence of stratospheric dynamics on the equator-to-pole contrast in tropopause height based on a simple energy balance model with a fixed tropospheric isentropic potential vorticity gradient. In general, the present analysis finds tropopause height modifications due to stratospheric dynamics on the order of the seasonal cycle or longer. On a global mean the mass of the troposphere is reduced in the SRE solution compared to the control run mainly due to the large reduction in tropical tropopause height. When the residual-circulation-induced heating is reintroduced [the stratospheric circulation–radiation (SCR) solution] as the dominant stratospheric dynamical contribution, the tropopause structure of the CCM is qualitatively recovered. Small discrepancies exist in the tropics and in the southern polar region.

It is important to note that the above findings do not diminish the role of tropospheric dynamics in setting the height of the tropopause. The equator-to-pole contrast in tropopause height is still on the order of a few kilometers in the SRE solution, which by definition cannot be due to stratospheric dynamics. Moreover, the change in tropopause height when going from a pure radiative equilibrium to a radiative–convective equilibrium is on the order of the tropopause height modifications due to stratospheric dynamics or larger (e.g., Manabe and Wetherald 1967). Furthermore, simple constraints that assume a stratosphere in radiative equilibrium, such as based on tropospheric lapse rate and surface temperature (Thuburn and Craig 1997) or on surface temperature and its meridional gradient (Schneider 2004), may still determine the tropopause height response to external perturbations (as shown by those authors in idealized GCM experiments). To what extent the stratospheric circulation may play a modifying role in these constraints, for example, in determining the tropopause height response to climate change (Son et al. 2009), remains an open question.

Concerning the lower stratospheric static stability structure, it is shown in the present study that the SRE solution does not contain a tropopause inversion layer (TIL) in the winter extratropics and has a much less pronounced tropical TIL than in the control run. The SCR solution, on the other hand, contains a TIL at all latitudes that closely resembles that of the CCM. This confirms the validity of the approximation in the heat budget, Eq. (2), in the present context. Stratospheric dynamics in the form of the residual circulation seem to play a dominant role in forming a TIL except for the polar regions during summer. The vertical structure of the vertical residual velocity is identified as the dominant forcing term [as confirmed by Miyazaki et al. (2010) in a high-resolution GCM simulation]. In midlatitudes, the annual cycle of maximum static stability just above the tropopause ($\overline{N^2}_{\max}$) follows the annual cycle of $-\partial_z \overline{w}^*|_{\max}$ with a time lag of 2–4 months. Simple arguments for this time lag are provided based on approximating radiative heating rates by simple Newtonian damping. Finally, it is shown that a midlatitudinal TIL can be obtained by replacing radiation in the SCR solution by simple Newtonian damping.

The TIL formation mechanism discussed here is consistent with the one speculated about in Birner et al. (2002) for midlatitudes in that subsidence within the downward branch of the stratospheric residual circulation plays a crucial role. It is furthermore interesting to note that the pivotal forcing term in the static stability budget, $-\partial_z(\overline{w}^*\overline{N^2})$, is formally equal to the one discussed in Wirth (2004) and Wirth and Szabo (2007) if $\overline{w}^*$ is replaced by the ageostrophic wind of upper-level disturbances. Since the residual circulation includes the averaged effect of many baroclinic life cycles with their embedded cyclones and anticyclones (and to the extent that they contribute to the Eliassen–Palm flux divergence *above* the tropopause) the mechanism discussed in Wirth (2004), Wirth and Szabo (2007), and A. R. Erler and V. Wirth (2009, unpublished manuscript) might be part of the mechanism discussed here. More research is required to clarify this.

The results of the present study highlight that, even though the TIL is a global phenomenon, its formation mechanisms involve different processes at different latitudes. In the polar region radiation seems to represent the dominant cause of the TIL, along the lines of Randel et al. (2007b) and Kunz et al. (2009) [although note that recent findings by Grise et al. (2010) suggest a significant stratospheric dynamical impact on interannual TIL variability in the polar regions during winter]. In midlatitudes large-scale dynamics, as represented by the residual circulation, seem dominant. In the tropics both radiation and circulation seem important. Similar balances between

radiation and residual circulation are seen in the CMAM and ERA-40 with some minor differences, mainly on a quantitative level. This suggests that mechanisms as found in CMAM carry over to reanalysis data and probably the real atmosphere.

Acknowledgments. Fruitful discussions with Michaela Hegglin and Ted Shepherd during the early stages of this work are gratefully acknowledged. James Anstey and Stephen Beagley provided technical help with the CMAM runs. Thanks to the thoughtful comments and constructive criticism by V. Wirth and two anonymous reviewers, as well as to comments by Anne Kunz, Paul Konopka, and Kevin Grise on an earlier version of the manuscript. TB's funding at the University of Toronto came through the Natural Sciences and Engineering Research Council and the Canadian Foundation for Climate and Atmospheric Sciences. Free access to ERA-40 data, originally generated by ECMWF, was provided through the National Center for Atmospheric Research.

APPENDIX A

Tropospheric Setup for Stratospheric Radiative Equilibrium Calculation

A stratosphere in radiative equilibrium leads to a lower tropopause in the tropics and a higher tropopause in the extratropics. In the tropical case, constraining the tropospheric temperature profile is straightforward: at each time step the tropopause is calculated and radiative temperature tendencies are only applied to levels above that tropopause. In the extratropics the rising tropopause, as the SRE solution is approached, is caused by radiative cooling at and above the level of the initial tropopause. This radiative cooling will in general tend to produce superadiabatic lapse rates in the region above the initial tropopause but below the tropopause in SRE. To prevent these superadiabatic lapse rates the following algorithm is applied each time step to preserve the shape of the initial (i.e., CMAM's) upper tropospheric lapse rate profile. First, temperature tendencies due to the clear-sky radiative heating rates, as computed by the CRM, are applied at each level above the level of maximum lapse rate z_0 (typically located around 500 hPa in the extratropics and around 300 hPa in the tropics). Then, an idealized profile of the vertical temperature gradient $\Gamma(z) = \partial_z T$ between z_0 and the tropopause is computed based on the assumption that the functional form of the mid to upper tropospheric profile of $\Gamma(z)$ can be approximated by a second-order polynomial:

$$\tilde{\Gamma}(z) = a_0 + a_1 z + a_2 z^2.$$

The coefficients a_i ($i = 0, 1, 2$) are obtained through the boundary conditions $\tilde{\Gamma}(z_0) = \Gamma(z_0)$ and $\tilde{\Gamma}(z_{\mathrm{TP}}) = \Gamma(z_{\mathrm{TP}})$, and the condition that $\tilde{\Gamma}(z_0)$ represents a minimum (i.e., $0 = 2a_2 z_0 + a_1$). The tropopause z_{TP} as used here is obtained by a two-step calculation. First, an interim tropopause is calculated as the level of maximum curvature in the temperature profile. The average lower stratospheric temperature gradient Γ_{str} is then computed (between the interim tropopause and ~25 km) and the final instantaneous tropopause is determined as the level above which Γ first exceeds Γ_{str}. This modified tropopause proved to represent a more robust estimate for the purpose of adjusting the tropospheric temperature profile at each time step. Finally, the temperature profile above z_0 is adjusted such that Γ does not exceed $\tilde{\Gamma}$ at any level. Figure A1 shows the resulting profiles of Γ over the tropics and northern midlatitudes for the SRE solution and CMAM (for DJF only). Evidently, the functional form of Γ as obtained from the SRE solution closely resembles the one from CMAM.

APPENDIX B

Idealized Functional Relationships for Θ_{rad} and τ_{rad}

Here Θ_{rad} is specified through a corresponding idealized distribution of $N^2_{\mathrm{rad}} = g\Theta^{-1}_{\mathrm{rad}}\partial_z\Theta_{\mathrm{rad}}$ with the boundary condition $\Theta_{\mathrm{rad}}(\varphi, z = z_{\mathrm{BC}}) = \bar{\Theta}(\varphi, z = z_{\mathrm{BC}})$, where z_{BC} is arbitrarily set to the model level just below 5 km, which represents a compromise between lying well below the tropopause but still above ground everywhere in the model.

Both N^2_{rad} and τ_{rad} are specified as idealized steplike functions of the general form

$$A(\varphi)\tanh\frac{z - z_{\mathrm{TP}}(\varphi)}{\Delta_{\mathrm{TP}}} + B(\varphi), \qquad \text{(B1)}$$

where $z_{\mathrm{TP}}(\varphi)$ is the tropopause height taken from the model and Δ_{TP} is the thickness of the transition from the value $B - A$ far below the tropopause to $A + B$ far above the tropopause. Here we set $\Delta_{\mathrm{TP}} = 1$ km, roughly corresponding to the model's vertical resolution around the tropopause. Then $A(\varphi)$ and $B(\varphi)$ determine tropospheric and stratospheric background values (denoted by subscripts t and s, respectively): $N^2_{\mathrm{t}} = B - A$ and $N^2_{\mathrm{s}} = B + A$ in the case of N^2_{rad}, and $\tau_{\mathrm{t}} = B - A$ and $\tau_{\mathrm{s}} = B + A$ in the case of τ_{rad}. For simplicity the tropospheric background values are set constant: $N^2_{\mathrm{t}} = 1 \times 10^{-4}\ \mathrm{s}^{-2}$ and $\tau_{\mathrm{t}} = 5$ days (these tropospheric background values

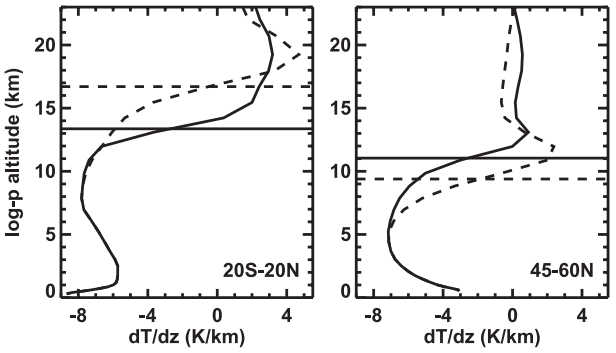

FIG. A1. Profiles of the vertical temperature gradient for the (left) tropics and (right) northern midlatitudes for DJF for the SRE solution (solid) and CMAM (dashed). Horizontal lines show corresponding tropopause heights.

are not crucial in this study as the focus is on the region just above the tropopause).

Stratospheric background radiative conditions differ between the tropics and extratropics and are further modified in polar night. This is accounted for by specifying steplike functions for N_s^2 and τ_s in latitude of the form

$$\begin{cases} C\tanh\dfrac{\varphi-\varphi_{0s}}{\Delta\varphi_s}+D, & \varphi<0 \\ C+D, & \varphi=0 \\ -C\tanh\dfrac{\varphi-\varphi_{0n}}{\Delta\varphi_n}+D, & \varphi>0. \end{cases} \quad \text{(B2)}$$

Here $\varphi_{0s,n}$ and $\Delta\varphi_{s,n}$ represent seasonally dependent tropics–extratropics transition latitudes and corresponding widths, $\varphi_{0s,n}$ are taken to be the latitudes of maximum $\partial_\varphi z_{TP}$ in the Northern (n) and Southern (s) Hemisphere, and $\Delta\varphi_{s,n}$ are arbitrarily set to 10° in the winter hemisphere and 15° in the summer hemisphere: $C = 1 \times 10^{-4}$ s^{-2} and $D = 5 \times 10^{-4}$ s^{-2} in the case of N_s^2, and $C =$ 10 days and $D = 40$ days in the case of τ_s.

To account for the reduced stratospheric stratification during polar night, N_{rad}^2 is further modified by a polar night factor f_{pn} that is 1 outside the polar stratosphere and reduces N_{rad}^2 by 25% toward the pole above 15 km:

$$f_{pn}=\frac{f_{pn}^{\varphi}-1}{2}\tanh\frac{z-z_{pn}}{\Delta z_{pn}}+\frac{f_{pn}^{\varphi}+1}{2}. \quad \text{(B3)}$$

Here $z_{pn} = 15$ km, $\Delta z_{pn} = 1$ km, and

$$f_{pn}^{\varphi}=\begin{cases} -\dfrac{1}{8}\tanh\dfrac{\varphi-\varphi_{pn}}{\Delta\varphi_{pn}}+\dfrac{7}{8} & \text{for DJF} \\ -\dfrac{1}{8}\tanh-\dfrac{\varphi-\varphi_{pn}}{\Delta\varphi_{pn}}+\dfrac{7}{8} & \text{for JJA,} \end{cases} \quad \text{(B4)}$$

with $\varphi_{pn} = 60°$N for DJF ($\varphi_{pn} = 60°$S for JJA) and $\Delta\varphi_{pn} = 10°$.

REFERENCES

Andrews, D. G., J. R. Holton, and C. B. Leovy, 1987: *Middle Atmosphere Dynamics*. Academic Press, 489 pp.

Beagley, S. R., J. de Grandpré, J. Koshyk, N. A. McFarlane, and T. G. Shepherd, 1997: Radiative–dynamical climatology of the first-generation Canadian Middle Atmosphere Model. *Atmos.–Ocean,* **35,** 293–331.

Bell, S. W., and M. A. Geller, 2008: Tropopause inversion layer: Seasonal and latitudinal variations and representation in standard radiosonde data and global models. *J. Geophys. Res.,* **113,** D05109, doi:10.1029/2007JD009022.

Bian, J., and H. Chen, 2008: Statistics of the tropopause inversion layer over Beijing. *Adv. Atmos. Sci.,* **25,** 381–386, doi:10.1007/s00376-008-0381-1.

Birner, T., 2006: Fine-scale structure of the extratropical tropopause region. *J. Geophys. Res.,* **111,** D04104, doi:10.1029/2005JD006301.

——, A. Dörnbrack, and U. Schumann, 2002: How sharp is the tropopause at midlatitudes? *Geophys. Res. Lett.,* **29,** 1700, doi:10.1029/2002GL015142.

——, D. Sankey, and T. G. Shepherd, 2006: The tropopause inversion layer in models and analyses. *Geophys. Res. Lett.,* **33,** L14804, doi:10.1029/2006GL026549.

Dell'Aquila, A., P. M. Ruti, and A. Sutera, 2007: Effects of the baroclinic adjustment on the tropopause in the NCEP–NCAR reanalysis. *Climate Dyn.,* **28,** 325–332, doi:10.1007/s00382-006-0199-4.

Egger, J., 1995: Tropopause height in baroclinic channel flow. *J. Atmos. Sci.,* **52,** 2232–2241.

Folkins, I., and R. V. Martin, 2005: The vertical structure of tropical convection and its impact on the budgets of water vapor and ozone. *J. Atmos. Sci.,* **62,** 1560–1573.

Frierson, D. M. W., I. M. Held, and P. Zurita-Gotor, 2006: A gray-radiation aquaplanet moist GCM. Part I: Static stability and eddy scale. *J. Atmos. Sci.,* **63,** 2548–2566.

Gabriel, A., G. Schmitz, and R. Geprägs, 1999: The tropopause in a 2D circulation model. *J. Atmos. Sci.,* **56,** 4059–4068.

Gettelman, A., and T. Birner, 2007: Insights into tropical tropopause layer processes using global models. *J. Geophys. Res.,* **112,** D23104, doi:10.1029/2007JD008945.

Grise, K. M., D. W. J. Thompson, and T. Birner, 2010: A global survey of static stability in the stratosphere and upper troposphere. *J. Climate,* **23,** 2275–2292.

Haynes, P., J. Scinocca, and M. Greenslade, 2001: Formation and maintenance of the extratropical tropopause by baroclinic eddies. *Geophys. Res. Lett.,* **28,** 4179–4182.

Hegglin, M. I., and Coauthors, 2006: Measurements of NO, NO_y, N_2O, and O_3 during SPURT: Implications for transport and chemistry in the lowermost stratosphere. *Atmos. Chem. Phys.,* **6,** 1331–1350.

——, C. D. Boone, G. L. Manney, and K. A. Walker, 2009: A global view of the extratropical tropopause transition layer from Atmospheric Chemistry Experiment Fourier Transform Spectrometer O_3, H_2O, and CO. *J. Geophys. Res.,* **114,** D00B11, doi:10.1029/2008JD009984.

Held, I. M., 1982: On the height of the tropopause and the static stability of the troposphere. *J. Atmos. Sci.,* **39,** 412–417.

——, and T. Schneider, 1999: The surface branch of the zonally averaged mass transport circulation in the troposphere. *J. Atmos. Sci.,* **56,** 1688–1697.

Highwood, E. J., and B. J. Hoskins, 1998: The tropical tropopause. *Quart. J. Roy. Meteor. Soc.,* **124,** 1579–1604.

Hoor, P., H. Fischer, L. Lange, J. Lelieveld, and D. Brunner, 2002: Seasonal variations of a mixing layer in the lowermost stratosphere as identified by the $CO–O_3$ correlation from in situ measurements. *J. Geophys. Res.,* **107,** 4044, doi:10.1029/2000JD000289.

Iwasaki, T., 1989: A diagnostic formulation for wave–mean flow interactions and Lagrangian-mean circulation with a hybrid vertical coordinate of pressure and isentropes. *J. Meteor. Soc. Japan,* **67,** 293–312.

Juckes, M., 2000: The static stability of the midlatitude troposphere: The relevance of moisture. *J. Atmos. Sci.,* **57,** 3050–3057.

——, 2001: A generalization of the transformed Eulerian mean meridional circulation. *Quart. J. Roy. Meteor. Soc.,* **127,** 147–160.

Kiehl, J. T., J. J. Hack, G. B. Bonan, B. A. Boville, B. P. Briegleb, D. L. Williamson, and P. J. Rasch, 1996: Description of the NCAR Community Climate Model (CCM3). NCAR Tech. Note NCAR/TN-420 + STR, 152 pp.

Kirk-Davidoff, D. B., and R. S. Lindzen, 2000: An energy balance model based on potential vorticity homogenization. *J. Climate,* **13,** 431–448.

Kunz, A., P. Konopka, R. Müller, L. L. Pan, C. Schiller, and F. Rohrer, 2009: High static stability in the mixing layer above the extratropical tropopause. *J. Geophys. Res.,* **114,** D16305, doi:10.1029/2009JD011840.

Manabe, S., and R. F. Strickler, 1964: Thermal equilibrium of the atmosphere with a convective adjustment. *J. Atmos. Sci.,* **21,** 361–385.

——, and R. T. Wetherald, 1967: Thermal equilibrium of the atmosphere with a given distribution of relative humidity. *J. Atmos. Sci.,* **24,** 241–259.

Miyazaki, K., S. Watanabe, Y. Kawatani, Y. Tomikawa, M. Takahashi, and K. Sato, 2010: Transport and mixing in the extratropical tropopause region in a high-vertical-resolution GCM. Part I: Potential vorticity and heat budget analysis. *J. Atmos. Sci.,* **67,** 1239–1314.

Pan, L. L., S. Solomon, W. Randel, J.-F. Lamarque, P. Hess, J. Gille, E.-W. Chiou, and M. P. McCormick, 1997: Hemispheric asymmetries and seasonal variations of the lowermost stratospheric water vapor and ozone derived from SAGE II data. *J. Geophys. Res.,* **102,** 28 177–28 184.

——, E. J. Hintsa, E. M. Stone, E. M. Weinstock, and W. J. Randel, 2000: The seasonal cycle of water vapor and saturation vapor mixing ratio in the extratropical lowermost stratosphere. *J. Geophys. Res.,* **105,** 26 519–26 530.

Randel, W. J., R. R. Garcia, and F. Wu, 2002: Time-dependent upwelling in the tropical lower stratosphere estimated from the zonal-mean momentum budget. *J. Atmos. Sci.,* **59,** 2141–2152.

——, D. J. Seidel, and L. L. Pan, 2007a: Observational characteristics of double tropopauses. *J. Geophys. Res.,* **112,** D07309, doi:10.1029/2006JD007904.

——, F. Wu, and P. Forster, 2007b: The extratropical tropopause inversion layer: Global observations with GPS data, and a radiative forcing mechanism. *J. Atmos. Sci.,* **64,** 4489–4496.

Rosenlof, K. H., 1995: Seasonal cycle of the residual mean meridional circulation in the stratosphere. *J. Geophys. Res.,* **100,** 5173–5191.

Schneider, T., 2004: The tropopause and the thermal stratification in the extratropics of a dry atmosphere. *J. Atmos. Sci.,* **61,** 1317–1340.

——, 2007: The thermal stratification of the extratropical troposphere. *The Global Circulation of the Atmosphere,* T. Schneider and A. H. Sobel, Eds., Princeton University Press, 47–77.

Scinocca, J. F., N. A. McFarlane, M. Lazare, J. Li, and D. Plummer, 2008: Technical note: The CCCma third-generation AGCM and its extension into the middle atmosphere. *Atmos. Chem. Phys.,* **8,** 7055–7074.

Son, S.-W., and L. M. Polvani, 2007: The dynamical formation of an extratropical tropopause inversion layer in a relatively simple general circulation model. *Geophys. Res. Lett.,* **34,** L17806, doi:10.1029/2007GL030564.

——, S. Lee, and S. B. Feldstein, 2007: Intraseasonal variability of the zonal-mean extratropical tropopause height. *J. Atmos. Sci.,* **64,** 608–620.

——, and Coauthors, 2009: The impact of stratospheric ozone recovery on tropopause height trends. *J. Climate,* **22,** 429–445.

Thuburn, J., and G. C. Craig, 1997: GCM tests of theories for the height of the tropopause. *J. Atmos. Sci.,* **54,** 869–882.

——, and ——, 2000: Stratospheric influence on tropopause height: the radiative constraint. *J. Atmos. Sci.,* **57,** 17–28.

——, and ——, 2002: On the temperature structure of the tropical substratosphere. *J. Geophys. Res.,* **107,** 4017, doi:10.1029/2001JD000448.

Uppala, S. M., and Coauthors, 2005: The ERA-40 Re-Analysis. *Quart. J. Roy. Meteor. Soc.,* **131,** 2961–3012.

Wirth, V., 2003: Static stability in the extratropical tropopause region. *J. Atmos. Sci.,* **60,** 1395–1409.

——, 2004: A dynamical mechanism for tropopause sharpening. *Meteor. Z.,* **13,** 477–484.

——, and T. Szabo, 2007: Sharpness of the extratropical tropopause in baroclinic life cycle experiments. *Geophys. Res. Lett.,* **34,** L02809, doi:10.1029/2006GL028369.

WMO, 1957: Meteorology—A three-dimensional science. *WMO Bull.,* **6,** 134–138.

Wong, S., and W.-C. Wang, 2003: Tropical–extratropical connection in interannual variation of the tropopause: Comparison between NCEP/NCAR reanalysis and an atmospheric general circulation model simulation. *J. Geophys. Res.,* **108,** 4043, doi:10.1029/2001JD002016.

Zängl, G., 2002: Dynamical heating in the polar lower stratosphere and its impact on the tropopause. *J. Geophys. Res.,* **107,** 4079, doi:10.1029/2001JD000662.

——, and V. Wirth, 2002: Synoptic-scale variability of the polar and subpolar tropopause: Data analysis and idealized PV inversions. *Quart. J. Roy. Meteor. Soc.,* **128,** 2301–2315.

Zhou, X. L., M. A. Geller, and M. H. Zhang, 2001: Tropical cold point tropopause characteristics derived from ECMWF reanalyses and soundings. *J. Climate,* **14,** 1823–1838.